

THE CAUSE OF CAUSAL EMERGENCE: REDISTRIBUTION OF UNCERTAINTY

Liye Jia^{1,2,4,6}, Cong Zhou^{1,2,4,6}, Ka Lok Man², Sheng-Uei Guan³, Jeremy Smith⁴, and Yutao Yue^{1,5,6}*

¹*Institute of Deep Perception Technology, JITRI, Wuxi 214000, China*

²*School of Advanced Technology, Xi'an Jiaotong-Liverpool University, Suzhou 215123, China*

³*Department of Computing, Xi'an Jiaotong-Liverpool University, Suzhou 215123, China*

⁴*Department of Electrical Engineering and Electronics, University of Liverpool, Liverpool L69 3BX, United Kingdom*

⁵*Department of Mathematical Sciences, University of Liverpool, Liverpool L69 3BX, United Kingdom*

⁶*XJTLU-JITRI Academy of Industrial Technology, Xi'an Jiaotong-Liverpool University, Suzhou 215123, China*

*Correspondence: yueyutao@idpt.org

December 6, 2022

ABSTRACT

It is crucial to choose the appropriate scale in order to build an effective and informational representation of a complex system. Scientists carefully choose the scales for their experiments to extract the variables that describe the causalities in the system. They found that the coarse scale(macro) is sometimes more causal and informative than the numerous-parameter observations(micro). The phenomenon that the causality emerges by coarse-graining is called Causal Emergence(CE). Based on information theory, a number of recent works quantitatively showed that CE indeed happens while coarse-graining a micro model to the macro. However, the existing works have not discussed the question of why and when the CE happens. We quantitatively analyze the redistribution of uncertainties for coarse-graining and suggest that the redistribution of uncertainties is the cause of causal emergence. We further analyze the thresholds that determine if CE happens or not. From the regularity of the transition probability matrix(TPM) of discrete systems, the mathematical expressions of the model properties are derived. The values of thresholds for different operations are computed. The results provide the critical and specific conditions of CE as helpful suggestions for choosing the proper coarse-graining operation. The results also provided a new way to better understand the nature of causality and causal emergence.

Keywords Granularity, Causal Emergence, Effective Information, Transition Probability Matrix, Coarse-graining, Uncertainty Redistribution, Causal Emergence Quantification Equation

1 Introduction

We create an informational representation of the physical world around us to survive, interpret and change it. The informational representation is often in the form of concepts (e.g., natural language words) or mathematical variables and their values (e.g., all forms of data). [1, 2] The world is not just a random collection of facts, but rather an interconnected complex network of facts. In this network, the phenomenon of causation can very often be observed. [3]

Surprisingly, many complex systems can be described by quite simple mathematical relations of just a few variables, all the way from quantum mechanics to macroeconomics. [4] The simplicity of these mathematical relations sometimes is the result of approximations (e.g., marginal revenue $\Delta MR = \frac{\Delta TR}{\Delta Q}$ in economics [5]), while sometimes seems to be intrinsic to the system (e.g., energy of a photon $E = h\nu$ in physics [6]). Causation naturally exists in these mathematical relations, e.g., if a physicist changes the value of frequency ν , the energy of the photon he or she measures would change accordingly.

In many cases, a well-defined mathematical relation is not available. Causation then needs to be interpreted from a statistical view of the data. For example, if one observes wet road after rain fall a few times, there is possibly a causal relationship between the two facts. If he or she observes it many times without exception, the causal relationship would be strong. Causation has long been widely discussed in many disciplines, such as philosophy, physics, and mathematics. [7, 8, 9, 10, 11, 12, 13, 14] However, the quantitative measure of the "strength" of causation has been seriously studied only since about a decade ago. [15]

In order to have an effective informational representation of a complex system, the granularity of study is a key. [2] For instance, if we want to investigate the phenomenon of human intelligence, we can study it at atomic level since everything including neurons and nerve cells are atoms, we can study it at molecular level (i.e., a group of atoms) by looking into the chemical reactions responsible for the regulation and function of brain activities, we can study it at cell level (i.e., a group of molecules) by looking into the different status of neuron cells, the electric signals transmitting among them, and the way they connect to one another, we can study it at all levels through minicolumns (i.e., a group of cells [16]), encephalic regions (e.g., V2 visual area is a group of minicolumns [17] [18]), and the whole cortex, the entire brain, etc. We can define different variables at different granularity levels of study, e.g., in the case of studying the air in a room, we can define momentum of each molecule ("micro" variable) or air temperature ("macro" variable). When we do "coarse-graining" by switching granularity from a micro level to a macro level, we lose part of the information.

The interesting and somewhat strange phenomenon of causal emergence arises when we investigate causation at different granularity levels. Sometimes, the causation of a system at the macro level is "higher" than micro level, or it seems there is no causation at micro level, but there is significant causation at macro level. In these cases, we say more causation "emerges" when we do coarse-graining, and there is a causal emergence (CE). CE has been widely discussed in a qualitative fashion [7, 9, 14]. For example, [14] categorizes emergence into four kinds, namely, simple (or nominal) emergence, weak emergence, multiple emergence, and strong emergence.

Erik Hoel and coworkers formally started the quantitative study of CE using the measure of causation called effective information (EI). In systems described by both discrete [15, 19] and continuous [4] variables, the phenomenon of CE was analyzed, the formulation of calculating the "amount of causal emergence" was mathematically given, and the exact values (in bits) were demonstrated in toy examples. Furthermore, it was shown that the phenomenon of CE stands while changing the measure of causation from EI to other methods. [20] In order to better understand CE, a recent work viewed CE as a form of information transformation, [21] which indeed helps a lot to understand CE, and in the meantime relies on the definition of the three different types of information. We consider these works as an important advancement in the study of CE and causation in complex systems.

Nevertheless, regardless of the extensive conceptual analysis and numerical calculations on the phenomenon of CE, it is far from clear exactly how CE happens, when it happens and when it does not. For example, all toy examples in previously mentioned works that demonstrated CE were artificially (and arbitrarily) chosen to prove and demonstrate the existence of CE, while the cases that CE does not happen were neglected. Furthermore, there are still debates and thus lacks a clear explanation on why even if CE can actually happen, since coarse-graining is an action of discarding part of the information. [21] These issues are hindering us from better understanding complex systems, all the way from social phenomena, psychological patterns, intelligent creatures, to various natural physical complex systems.

In this work, we carefully analyze the quantitative critical conditions of CE, give corresponding mathematical expressions, and propose that the cause of CE is the redistribution of uncertainty in the system. In Section 2, we display the experimental tool and equations derived from the materials in several existing papers. In section 3, we provide the experimental result to prove the main point of this work. In section 4, we discuss possible methods to push the study of CE conditions forward. In section 5, we summarize the contributions of this paper and future possible improvements.

2 Materials & Methods

2.1 Fundamental Theory: Effective Information(EI) and Causal Emergence(CE)

Based on Judea Pearl's perturbational framework of causal analysis, Hoel et al proposed to quantify the system causality with Effective Information(EI), namely, the metric of the model's accuracy and interpretability[12][15][22]. They utilized the KL Divergence(D_{KL}) to measure the probability distribution of model's state transitions by Causal Information and Effect Information. Hereafter, EI is determined by three model attributes: Determinism, Degeneracy, and number of states N , as shown in Equation 1[15]. Determinism coefficient, derived by Effect Information, represents the confidence of the system's next stages given the current state. Degeneracy coefficient, sourced from Causal Information, indicates the explainability of the precise cause of the next stages. CE is introduced to describe the gain of a model's EI, when the model is squeezed by reducing the number of total states. In the rest of this paper, the original

model is named as the micro model, while the squeezed model is named as the macro model.

$$\begin{aligned} EI &= Effectiveness * \log_2(N) \\ &= (\text{Determinism coefficient} - \text{Degeneracy coefficient}) * \log_2(N) \end{aligned} \quad (1)$$

The issue is, the original calculation method of Determinism and Degeneracy is computationally intensive. Later, Hoel simplified the computation process of these two coefficients in Equation 1 by using the system's transition probability matrix(TPM). The TPM in Figure 1 is the quantitative representation of the model's Markov Chain. The row in the matrix shows all possible current states, and the column presents the future states. By checking the TPM, transition probability from the current state to all potential future states can be acquired. For Equation 2, the $do(S = s_{ij})$ specifies that the probability of the current state s_{ij} chosen from model's all potential interventions I_D . The conditional probability distribution $p(S_F|do(S = s_{ij}))$ is retrieved by checking the TPM's row captioned with s_{ij} . H^{max} represents the Maximum Entropy Distribution of the model's current states S . The determinism is the average KL Divergences(D_{KL}) between all possible $p(S_F|do(S = s_{ij}))$ and H^{max} normalized by $\log_2(N)$. For Equation 3, U_D denotes the model's effective distribution, which can also be gained from the TPM. The degeneracy is KL Divergence between U_D and I_D normalized by $\log_2(N)$. With this novel algorithm, Hoel managed to reproduce CE in his coarse-graining experiments. The limitation is, this algorithm can only be applied to models with discrete states, while in practice, many models tend to have continuous states.

$$determinism = \frac{1}{N} \sum_{do(s_{ij}) \in I_D} \frac{D_{KL}(p(S_F|do(S = s_{ij}))||H^{max})}{\log_2(N)} \quad (2)$$

$$degeneracy = \frac{D_{KL}(U_D||I_D)}{\log_2(N)} \quad (3)$$

In 2021, Hoel and Chvykov casually quantified continuous models by developing the EI_g algorithm based on Information Geometry Theory[4][23]. EI_g can be calculated by Equation 4, where V_I represents the volume of the intervention manifold, and $\langle l(\theta) \rangle_I$ expresses the causation lost when modeling the system[4]. Following the Fisher Information Matrices, $h_{\mu\nu}$ quantifies the intervention manifold, and $g_{\mu\nu}$ measures the effect manifold. The drawback is, the computational complexity of Fisher Information Matrices hinders the EI_g implementation. For one-variable models, EI_g can be approximated by Equation 5, where θ denotes the model's variable, δ is the noise that influences the mapping from the intervention to θ , and ϵ indicates the noise of mapping from θ to the final effect, which makes the causal measurement for the one-variable continuous scenario more practical[4].

$$EI_g = \log \left[\frac{V_I}{(2\pi e)^{d/2}} \right] - \langle l(\theta) \rangle_I \quad (4)$$

$$\text{with } l(\theta) = \frac{1}{2} \log \det (\mathbf{1} + g_{\mu\nu}^{-1} h_{\mu\nu})$$

$$EI_{approx} \simeq -\frac{1}{2} \int d\theta \log \left[2\pi e \left(\left(\frac{\epsilon}{f'(\theta)} \right)^2 + \delta^2 \right) \right] \quad (5)$$

a	00	01	10	11
	00	01	10	11
00	0	1	0	0
01	0	0	1	0
10	0	0	0	1
11	1	0	0	0

b	00	01	10	11
	00	01	10	11
00	0.09	0.81	0.01	0.09
01	0.09	0.01	0.81	0.09
10	0.01	0.09	0.09	0.81
11	0.81	0.09	0.09	0.01

Figure 1: Transition Probability Matrix(TPM) of a Four-State(Two-Variable) Discrete Model. (a) is an example of a deterministic model's TPM. (b) is an example of a stochastic model's TPM.

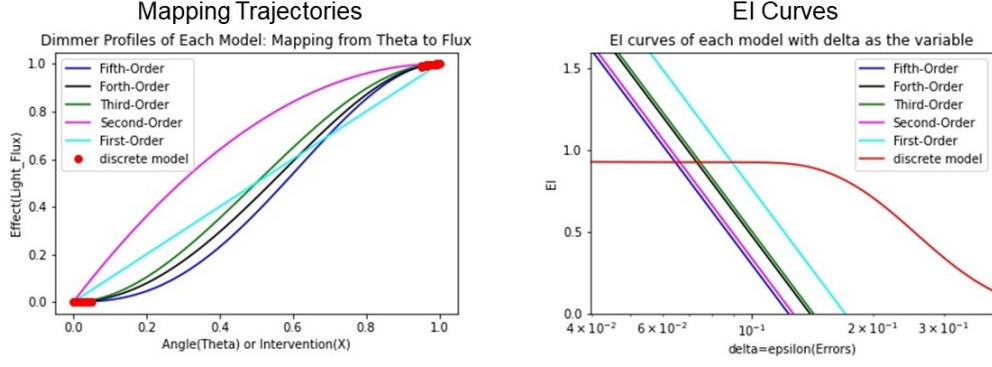


Figure 2: Six Continuous Models' Mapping Trajectory and Their Corresponding EI Curves. The left graph shows five continuous and one discrete mapping trajectories generated by the polynomials, which their highest orders are listed in the legend. The right graph is each trajectory's EI related to the errors calculated by Equation 5.

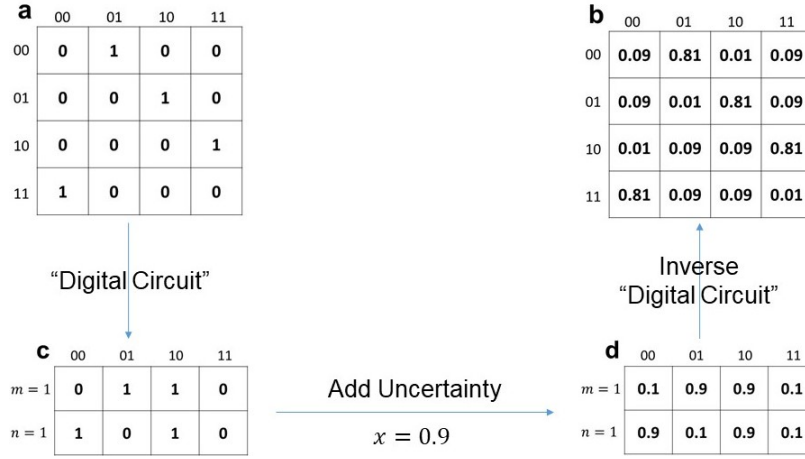


Figure 3: TPM Generator's Process. The variable dynamics (c) is derived by the deterministic TPM through the "digital circuit" process. 1 elements in (c) are replaced by x , and 0 elements are substituted by $1 - x$. With the probabilist variable dynamics (d), the stochastic TPM (b) is calculated by inverse "digital circuit" process.

To sum up, Hoel discovered the CE by estimating the EI of both discrete and continuous models[4][15][19]. Figure 2 shows our reproduced six mapping trajectories of one-variable models and their corresponding EI curves. To the best of our knowledge[24][25], the specific conditions for CE have not been discussed in academic papers. This paper aims to prove that uncertainty redistribution is a significant factor of the CE by coarse-graining operations.

2.2 Experiment Tool: General EI Calculator

Based on Equations 1, 2, and 3, we created the General EI Calculator to verify our assumption and plot the relationship between the discrete model's EI and uncertainties. This calculator has three components: Hyperparameter Adjustor, TPM Generator, and EI Meter. There are three hyperparameters: n , $future_dg_num$, and dg_level . The n indicates the number of the model's total states. The $future_dg_num$ and dg_level determine the model's degeneracy. Based on three hyperparameters above, TPM Generator can produce the stochastic TPM with the uncertainty x accordingly. Finally, EI Meter obtains the EI value from the generated TPM.

As shown in Figure 3, TPM Generator contains three processes: Digital Circuit, Add Uncertainty, and Inverse Digital Circuit. The assumption is, the model's states are sourced from the values of n -th binary variables, where the relationship between the total state number N and the number of model's binary variables n is $N = 2^n$. Digital Circuit represents the building process of the variable dynamics matrix by utilizing the 1 element positions of the deterministic TPM. For example, matrix (a) is the deterministic TPM of a four-state model, which has two binary variables m and n , and matrix (c) presents the probabilities of $m = 1$ and $n = 1$ given the current state s_{ij} . For transferring matrix (c) to matrix (d),

the specific uncertainty x is introduced by Add Uncertainty, in specific, we replace 1 and 0 elements of (c) with x and $1 - x$ respectively, and in this example, we let $x = 0.9$. Inverse Digital Circuit denotes the calculation to reproduce the stochastic TPM by the dynamics. Algorithms 1 and 2 describe the process of Digital Circuit and Inverse Digital Circuit.

Algorithm 1: Digital Circuit Process.

```

for "l" element positions of the TPM do
  if position represents the future state "ln" then
    | One element of first row of dynamics matrix is "1";
  end
  if position represents the future state "ml" then
    | One element of second row of dynamics matrix is "1";
  else
    | Other dynamics elements are "0";
  end
end

```

Algorithm 2: Inverse Digital Circuit Process.

Probabilities $p(s_F|s_{ij})$ of each future state s_F given the current state s_{ij} ;

```

for each  $s_{ij}$  represented by columns of the dynamics do
  |  $p(s_F = 00|s_{ij}) = [1 - p(m = 1|s_{ij})] * [1 - p(n = 1|s_{ij})]$ ;
  |  $p(s_F = 01|s_{ij}) = [1 - p(m = 1|s_{ij})] * p(n = 1|s_{ij})$ ;
  |  $p(s_F = 10|s_{ij}) = p(m = 1|s_{ij}) * [1 - p(n = 1|s_{ij})]$ ;
  |  $p(s_F = 11|s_{ij}) = p(m = 1|s_{ij}) * p(n = 1|s_{ij})$ ;
end

```

2.3 Finding: Causal Emergence Quantification Equation(CEQE)

After the derivation of the tested model's TPM, the model's determinism depends on the uncertainty exclusively, as described in Proposition 1.

Proposition 1. *The model's determinism only relates to the uncertainty x , as shown in Equation 6.*

$$\text{determinism} = 1 + (1 - x) \log_2(1 - x) + x \log_2(x) \quad (6)$$

Equation 6 is derived by the general regularity of the TPM's distribution by rows: each row contains the same elements with different layouts. Based on the TPM Generator's process in Figure 3, the TPMs of the two-variable model and three-variable model are produced as an example of the row's regularity. M_2 and M_3 are the generated stochastic TPM in which elements are represented with x polynomials.

$$M_2 = \begin{bmatrix} x(1-x) & x^2 & (1-x)^2 & x(1-x) \\ x(1-x) & (1-x)^2 & x^2 & x(1-x) \\ (1-x)^2 & x(1-x) & x(1-x) & x^2 \\ x^2 & x(1-x) & x(1-x) & (1-x)^2 \end{bmatrix}$$

$$M_3 = \begin{bmatrix} x^2(1-x) & x^3 & \cdots & (1-x)^3 & x(1-x)^2 \\ x^2(1-x) & x(1-x)^2 & \cdots & x^2(1-x) & x(1-x)^2 \\ \vdots & \vdots & \ddots & \vdots & \vdots \\ (1-x)^3 & x(1-x)^2 & \cdots & x^2(1-x) & x^3 \\ x^3 & x^2(1-x) & \cdots & x(1-x)^2 & (1-x)^3 \end{bmatrix}$$

The regularity is, M_2 's each row has one $(1-x)^2$, two $x(1-x)$, and one x^2 , and M_3 's each row includes one $(1-x)^3$, three $x(1-x)^2$, three $x^2(1-x)$, and one x^3 . This regularity also exists in TPMs for other models with 4-11 binary variables. In each row, the numbers of $x^{a-1}(1-x)^{n-(a-1)}$ and $x^{n-(a-1)}(1-x)^{a-1}$ are same, where n

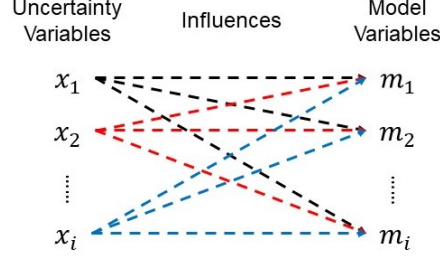


Figure 4: How the Uncertainty Variables Influence Model Variables. In our assumption, one uncertainty can influence multiple variables of the model, but one model's variable merely has one uncertainty.

indicates the amount of variables, and a is the order coefficient of the polynomial. Based on the regularities of different models' TPMs, we represented a general set of the distribution by rows E_D , where (Num) implies the number of same polynomials contained by the distribution:

$$E_D = \left\{ (1-x)^n, \dots, (Num) x^{n-(a-1)}(1-x)^{a-1}, (Num) x^{a-1}(1-x)^{n-(a-1)}, \dots, x^n \right\}$$

$$\text{where } Num = \prod_{m=1}^{a-1} \frac{n-m+1}{m} \quad (7)$$

The difference among these distributions by rows is the layouts of the elements in E_D . The layout differences do not influence the value of KL Divergence between the E_D and Maximum Entropy Distribution H^{max} . Therefore, the mathematical relationship between $D_{KL}(E_D||H^{max})$ and the uncertainty x can be expressed by Equation 8.

$$\begin{aligned} D_{KL}(E_D||H^{max}) &= E_D \cdot \log_2 \left(\frac{E_D}{H^{max}} \right) = \sum_{p_i \in E_D} p_i \cdot \log_2 \left(\frac{p_i}{\frac{1}{2^n}} \right) \\ &= n[1 + (1-x) \log_2(1-x) + x \log_2(x)] \end{aligned} \quad (8)$$

In Equation 2, $p(S_F|do(S = s_{ij}))$ represents the conditional probability distribution of future states S_F given the current state s_{ij} , and it can be derived by checking the distribution of the TPM's row. Therefore, this conditional distribution is equivalent to E_D , expressed by the equation $p(S_F|do(S = s_{ij})) = E_D$. With the relationship between the number of states N and the number of variables n , $N = 2^n$, Equation 2 can be adapted to the new parameters in form of a new formula below, and it can be simplified to Equation 6 about the uncertainty x following Equation 8. This general expression proves our Proposition 1: the model's determinism is barely influenced by the uncertainty.

$$\begin{aligned} determinism &= \frac{1}{2^n} \sum \frac{D_{KL}(E_D||H^{max})}{n} \\ &= 1 + (1-x) \log_2(1-x) + x \log_2(x) \end{aligned} \quad (9)$$

For models with multiple uncertainty variables, the regularity of the distribution by rows also exists in the TPMs. As shown in Figure 4, we only consider the situation that one model's variable is just influenced by one uncertainty variable, and the maximum number of uncertainties is four. For example, x_1 and x_2 separately influence each variable of the two-variable dynamics and one or two variables of the three-variable dynamics. In this situation, the TPMs M_2 and M_3 transfer to M'_2 and M'_3 , which elements are polynomials with x_1 and x_2 .

$$M'_2 = \begin{bmatrix} x_1(1-x_2) & x_1x_2 & (1-x_1)(1-x_2) & (1-x_1)x_2 \\ (1-x_1)x_2 & (1-x_1)(1-x_2) & x_1x_2 & x_1(1-x_2) \\ (1-x_1)(1-x_2) & (1-x_1)x_2 & x_1(1-x_2) & x_1x_2 \\ x_1x_2 & x_1(1-x_2) & (1-x_1)x_2 & (1-x_1)(1-x_2) \end{bmatrix}$$

$$M'_3 = \begin{bmatrix} x_1^2(1-x_2) & x_1^2x_2 & \dots & (1-x_1)^2(1-x_2) & (1-x_1)^2x_2 \\ x_1(1-x_1)x_2 & x_1(1-x_1)(1-x_2) & \dots & (1-x_1)x_1x_2 & (1-x_1)x_1(1-x_2) \\ \vdots & \vdots & \ddots & \vdots & \vdots \\ (1-x_1)^2(1-x_2) & (1-x_1)^2x_2 & \dots & x_1^2(1-x_2) & x_1^2x_2 \\ x_1^2x_2 & x_1^2(1-x_2) & \dots & (1-x_1)^2x_2 & (1-x_1)^2(1-x_2) \end{bmatrix}$$

M'_2 's each row contains four kinds of polynomials with x_1 and x_2 , and there are six kinds of polynomials for M'_3 's row distribution. Since this regularity is common for the TPM of the model with n variables, Equation 10 gives the general expression of the model's determinism, where a_i is the constant that indicates the number of variables influenced by one of the uncertainties x_i . In form of this mathematical equation, Proposition 2 describes the model's EI varying degree following the multiple and independent uncertainties.

Proposition 2. *One of multiple uncertainties x_i 's effect on the model's EI attenuates to $\frac{a_i}{n}$ of the unified uncertainty x 's effect, where $x_i \in X$, and X is the set of total uncertainty variables.*

$$\text{determinism} = 1 + \sum_{i=1}^n \frac{a_i[(1 - x_i) \log_2(1 - x_i) + x_i \log_2(x_i)]}{n} \quad (10)$$

By replacing the determinism calculation in Equation 1 with Equation 6, the Causal Emergence Quantification Equation (CEQE) can quantify the uncertainty condition of CE when coarse-graining a n -variable stochastic model to the target EI , as shown in Equation 11. However, finding the exact value of x in Equation 11 is computationally intensive. Therefore, we propose Algorithm 3 to find the approximate value of x .

$$1 + (1 - x) \log_2(1 - x) + x \log_2(x) = \frac{EI}{n} \quad (11)$$

Algorithm 3: The Searching for Approximate Solution of the CEQE. The error of the solving approximation is less than 10^{-6} .

```

while  $| [1 + (1 - x_i) \log_2(1 - x_i) + x_i \log_2(x_i)] - \lfloor \frac{EI}{n} \rfloor | > T_c$  do
    if  $[1 + (1 - x_i) \log_2(1 - x_i) + x_i \log_2(x_i)] - \lfloor \frac{EI}{n} \rfloor > T_c$  then
        increase the value at the current decimal place;
    else
        go to the next decimal place;
    end
end

```

3 Results

3.1 Experiment 1: Causal Emergence After Fixed Coarse-graining or Flexible Coarse-graining Process

In [19], while Hoel specified the CE related to the coarse-graining choice, the uncertainty's influences are ignored. In this paper, we use the General EI Calculator to plot the EI curves of discrete models whose number of variables ranges from 1 to 11. When the model has one variable, EI is always 1 according to [4]. Based on the coarse-graining experiment results, we identified the threshold of uncertainty influences that will cause the CE. In this experiment, we define there are two coarse-graining categories: Hard Coarse-graining and Flexible Coarse-graining. Hard Coarse-graining is the operation that shrinks the original micro model to the one-variable macro model regardless of how many variables the original model has. Flexible Coarse-graining is the operation in which number of targeted model's variables can be manually set as long as it is less than the original model's number of variables.

For Hard Coarse-graining, we obtain the micro and macro EI related to the unified uncertainty magnitude $-\log_2(x)$, as Figure 5(a) shows. The CE uncertainty thresholds are presented by the intersections between the curves and the red straight line, which represents the EI of micro models and the one-variable model respectively. In Figure 5(b), the values of thresholds grows as the number of the original model's variables increases. Since the EI of the one-variable macro model is always 1, the target in Equation 11 is always 1, and the original model's variable range from 2 to 11. Based on Algorithm 3, the approximate values of uncertainty thresholds that constrain the CE through the Hard Coarse-graining are yielded, as shown in Figure 6. The result of Hard Coarse-graining experiment proves the existence of the CE uncertainty thresholds, and Proposition 3 summarizes the findings in this experiment.

Proposition 3. *The necessary condition of CE with Hard Coarse-graining is, the uncertainty magnitude of the original micro model has to exceed the CE uncertainty threshold.*

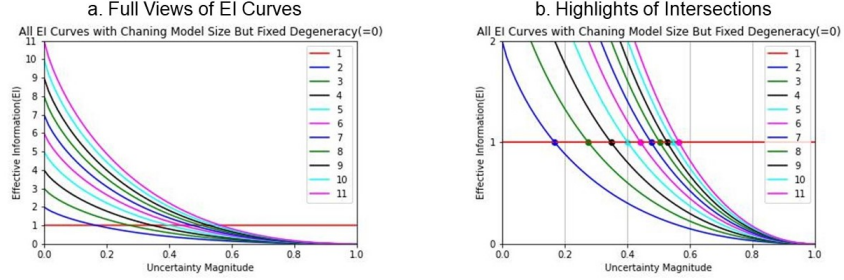


Figure 5: EI Curves and CE Thresholds. The full views of EI curves are the evidence to describe the CE that happens when the uncertainty is more significant than the intersections. The right provides more details of the thresholds to highlight our Proposition 3.

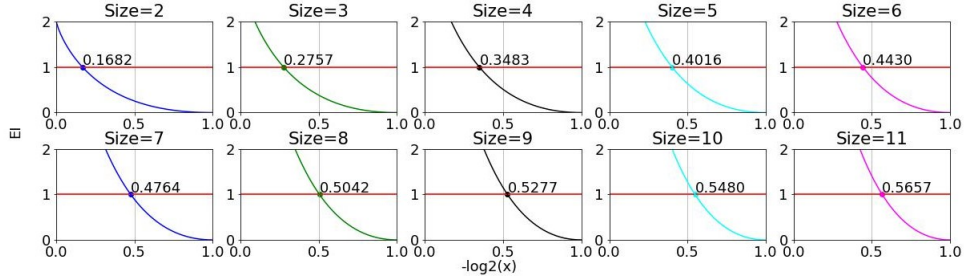


Figure 6: Specific Values of CE Threshold of Every Coarse-graining Operations. These results give the explicit values for the threshold that the uncertainty should exceed if the CE happens with the Coarse-graining. It is also comprehensible to verify our CEQE is general to quantify the CE uncertainty condition for any mapping operations.

For Flexible Coarse-graining, we prove the CE's essential factor is the redistribution of uncertainty based on the mathematical results. Since the EI of Flexible Coarse-graining target is also influenced by the uncertainty, we assume there is the fixed uncertainty x_f that cannot be decreased by the variable-squeezing operations, and the particular CEQE in Equation 12 to quantify the threshold value of x_f is that:

$$1 + (1 - x_f) \log_2(1 - x_f) + x_f \log_2(x_f) = \frac{n_o[1 + (1 - x_f) \log_2(1 - x_f) + x_f \log_2(x_f)]}{n_t} \quad (12)$$

In this provement, the micro model has three variables, and the macro model contains two variables. Therefore, following $n_o = 3$ and $n_t = 2$, Equation 12 can be simplified to the equation $\frac{1 + (1 - x_f) \log_2(1 - x_f) + x_f \log_2(x_f)}{1 + (1 - x_f) \log_2(1 - x_f) + x_f \log_2(x_f)} = \frac{n_o}{n_t} \Rightarrow 1 = \frac{3}{2}$, which is a false proposition. Therefore, the fixed uncertainty x_f cannot make the CEQE established. This result verifies the regularity that the Flexible Coarse-graining has to change the original uncertainty for the CE.

In Figures 7 and 8, there are two kinds of uncertainty thresholds: Absolute Threshold and Equivalent Threshold. Absolute Threshold is the rigorous constraint for the CE. To make the CE by Flexible Coarse-graining, the original micro model's uncertainty must transcend the Absolute Threshold. In Figure 7, three-variable model's uncertainty magnitude has to be greater than Absolute Threshold 0.0916. Equivalent Threshold provides the range of target model's uncertainty that the origin is redistributed to. In Figure 8, for the original micro model's EI with the uncertainty whose magnitude is 0.25, as the straight cyan line illustrates, Equivalent Threshold is 0.1433, which represents the targeted uncertainty range $[0, 0.1433)$ where the original uncertainty is redistributed to make the CE happen by Flexible Coarse-graining.

In Hard Coarse-graining experiments, the one-variable macro model's uncertainty magnitude is always 0 according to [4]. Therefore, squeezing the micro model with uncertainty that satisfies the uncertainty threshold in Figure 6 also brings the CE by the distribution of the original uncertainty. In this regard, Proposition 4 concludes the uncertainty condition that coarse-graining operations have to satisfy for the CE based on the experiment results of Hard and Flexible Coarse-graining.

Proposition 4. *By coarse-graining, the CE will happen when satisfies both of two conditions:*

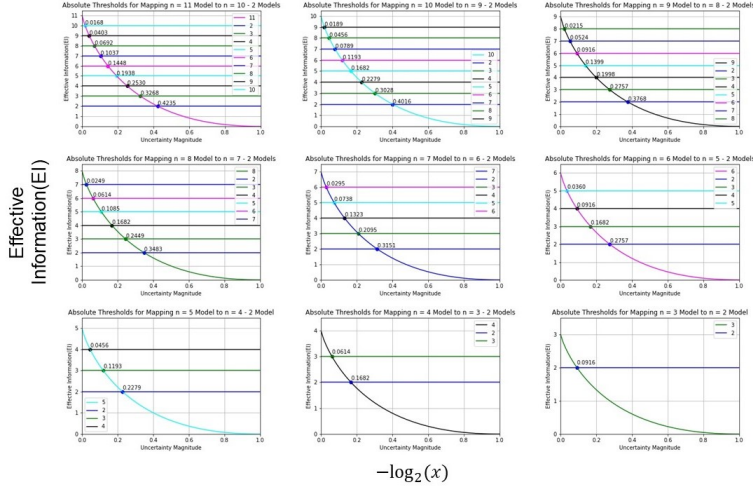


Figure 7: Absolute Thresholds as the Condition of the Uncertainty of Original Models. It is the first condition that the original uncertainty has to be larger than the threshold value to bring the CE from the Partial Coarse-graining.

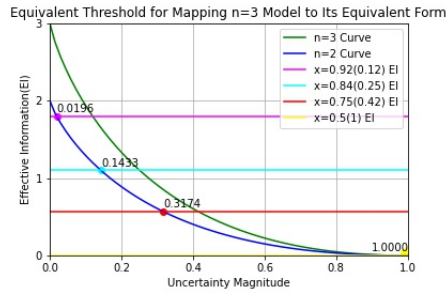


Figure 8: Equivalent Thresholds as the Condition of the Uncertainty Range that Operations Map To. Here, we use partially coarse-graining the three-variable model to the two-variable as an example. When the origin has 0.92 uncertainty(that means the magnitude is 0.12), the mapping uncertainty range is $[0, 0.0196)$. The range is $[0, 1)$ while the uncertainty attains the maximization(0.5, which is 1 uncertainty magnitude).

1. The uncertainty magnitude of original micro models has to exceed the value of CE uncertainty thresholds.
2. The uncertainty redistribution happens when the original micro model is squeezed to the target macro model.

3.2 Experiment 2: Effects of Multiple and Independent Uncertainties On the Model's EI

In this experiment, we visualized Proposition 2 by Figures 9 and 10. As an example of the two-variable model with multiple uncertainty variables, the model's deterministic TPM and variable dynamics are shown in Figure 3(a) and Figure 3(c), and M'_2 indicates the algebraically stochastic TPM with two uncertainty variables x_1 and x_2 . Figure 9 shows the model's EI that changes with both uncertainty variables increasement. (b) and (c) are the left and right projections of the 3D surface in (a), which represent the reduction of the model's EI with one of uncertainty variables, x_1 or x_2 . To highlight the attenuation of x_1 or x_2 's influences on the model's EI, Figure 10 displays the 2D curves that the two-variable model's EI decreases as x_1 , x_2 , or x_u changes independently. Figure 10(a) and (b) are 2D views of Figure 9(b) and Figure 9(c) respectively. ΔEI_1 and ΔEI_2 of total curves in the subfigures (a) and (b) are half of ΔEI_u of the blue curve in the subfigure (c), which means that $d_{x_i} EI = \frac{1}{2} d_{x_u} EI$, where $x_i \in X$ indicates one of multiple uncertainty variables, and x_u is the unified uncertainty variable. This result proves our Proposition 2: for one uncertainty variable $x_i \in X$, its effect on the model's EI attenuates to $\frac{\alpha_i}{n}$ of the effect of the unified uncertainty x_u . We can replace the calculation of determinism in Equation 1 with Equation 10 to quantify the CE uncertainty threshold for

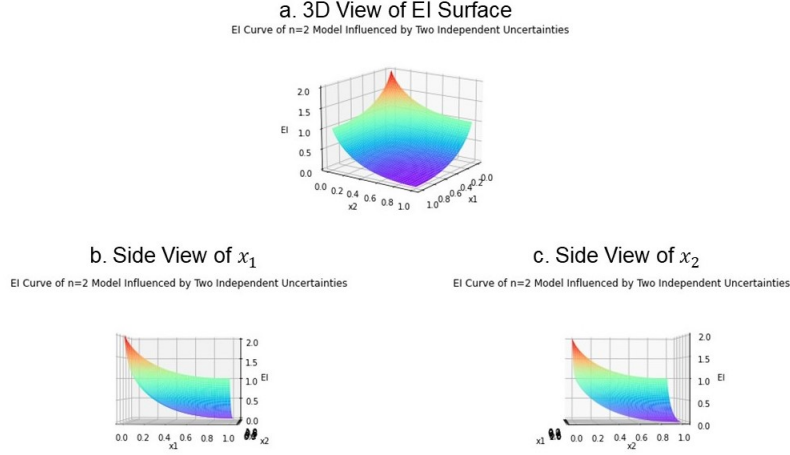


Figure 9: Two-Variable Model's EI with Multiple Uncertainties x_1 and x_2 . (a) is the 3D surface that displays the EI influenced by both uncertainty variables. (b) and (c) are the 3D surface's side views that show the influences of one uncertainty variable, x_1 or x_2 .

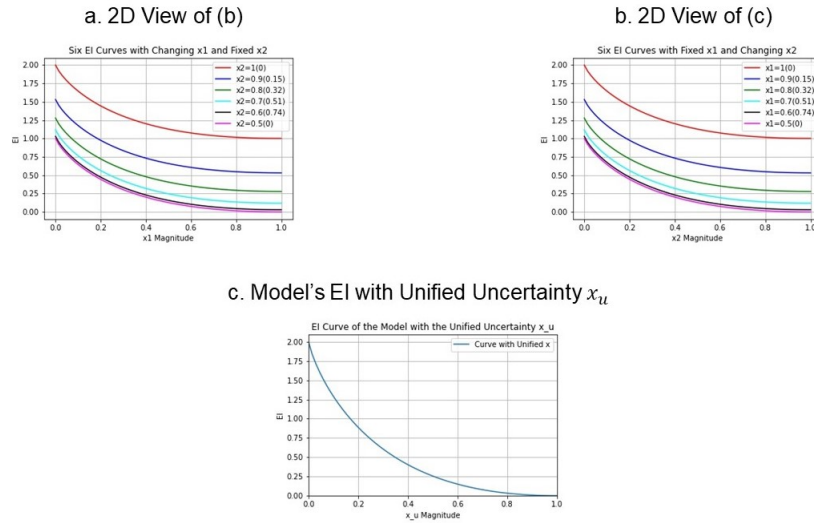


Figure 10: Two-Variable Model's EI with One of Multiple Uncertainty Variables, x_1 or x_2 , and with the Unified Uncertainty x_u . (a) and (b) are the 2D EI curves that illustrate the influences of x_1 or x_2 when another variable is fixed. (c) is the 2D curve of model's EI with unified uncertainty x_u .

the model with multiple uncertainties by Equation 13.

$$1 + \sum_{i=1}^n \frac{a_i [(1 - x_i) \log_2(1 - x_i) + x_i \log_2(x_i)]}{n} = \frac{EI}{n} \quad (13)$$

3.3 Experiment 3: The Boundary and Influences of the Degeneracy

As the model's explainability coefficient, the degeneracy is also a factor of the CE by coarse-graining operations. In Equation 11 and 13, we ignored the effect of degeneracy and assumed *degeneracy* = 0. To quantify the CE conditions and CE uncertainty thresholds influenced by the degeneracy coefficient, Equation 11 replaces the *determinism* in Equation 1, which *degeneracy* is not zero, to derive Equation 14.

$$[1 + (1 - x) \log_2(1 - x) + x \log_2(x)] - \text{degeneracy} = \frac{EI}{n} \quad (14)$$

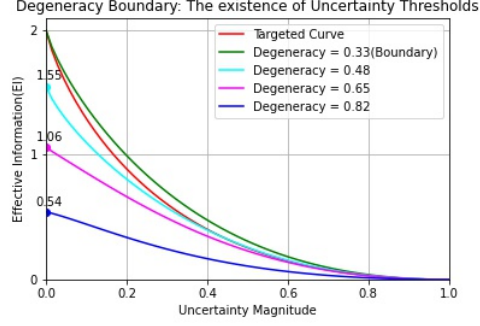


Figure 11: CE Degeneracy Boundary of the CE by Coarse-graining a Three-variable Micro Model to the Two-Variable Macro Model. Target Curve represents the EI of the macro model, and other curves are the EI of the micro models with different degeneracy.

Figure 11 illustrates the CE Degeneracy Boundary calculated by Equation 14. The CE degeneracy boundary is the micro model degeneracy's specific value, which diminishes the CE uncertainty thresholds since the maximum EI of the original micro model is less than the targeted macro model's maximum EI. In Figure 11, when $determinism = 1$, $EI = 2$, and $n = 3$, the CE degeneracy boundary is $degeneracy = \frac{1}{3}$ according to Equation 14, as the green curve displays. There is a situation that the EI of the micro model is greater than the macro model, as shown by the green curve and red curve. Therefore, we proposed the first degeneracy condition of CE after the coarse-graining: the original micro model's degeneracy is in the range (*CE Degeneracy Boundary*, 1].

Figure 12 shows the CE uncertainty thresholds when the micro model's degeneracy has not exceeded the CE degeneracy boundary. In this experiment, the model's degeneracy value is extracted from the General EI Calculator's EI Meter process. The intersections between curves and the straight line move to the left of the diagram following the degeneracy growth. This result presents that the CE uncertainty threshold decreases as the degeneracy increases. Proposition 5 recapitulates the CE conditions when the model's degeneracy is not zero.

Proposition 5. *If the micro model's degeneracy is not zero, the CE will happen under one of the following conditions:*

1. *The micro model's degeneracy $\in (CE\ Degeneracy\ Boundary, 1]$, and its uncertainty magnitude $\in [0, 1]$.*
2. *The micro model's degeneracy $\in [0, CE\ Degeneracy\ Boundary]$, and its uncertainty magnitude $\in (CE\ Uncertainty\ Threshold, 1]$.*

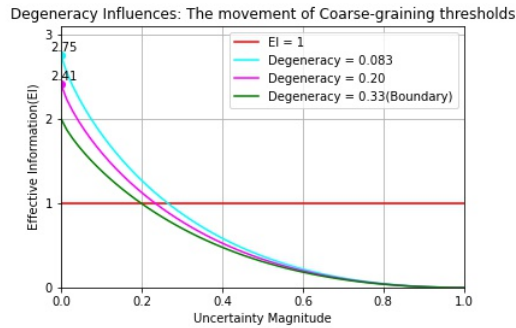


Figure 12: Degeneracy Influences on the CE uncertainty Thresholds. With different degeneracy values, the three-variable micro models are squeezed to the one-variable model, where curves represent the micro model's EI with the uncertainty, and the straight line is the one-variable model's $EI = 1$.

4 Discussions

4.1 Find Degeneracy Expression

Since the General EI Calculator's computational complexity is $O(2^n)$, the calculation of CE uncertainty thresholds by Equation 14 is expensive when the models have a large number of variables n . Therefore, the general degeneracy expression is desired to decline the computational intensity for solving the CEQE by Algorithm 3. For deriving the degeneracy expression that contains the uncertainty x and hyperparameters, $future_dg_num$ and dg_level , we propose two potential solutions: the Algebraic Method and the Numerical Method.

4.1.1 Algebraic Method

Algebraic Method aims to produce the degeneracy expression by the general regularity of the TPM's distribution by column. In this process, the TPM's transposition can help find the regularity by columns. For example, when $future_dg_num = 1$ and $dg_level = 2$, M_d represents the two-variable model's TPM with the corresponding degeneracy.

$$M_d = \begin{bmatrix} 0 & 1 & 0 & 0 \\ 0 & 0 & 1 & 0 \\ 0 & 0 & 0 & 1 \\ 0 & 1 & 0 & 0 \end{bmatrix}$$

Summing by the M_d 's columns, the dg_vector of M_d is $[0, 2, 1, 1]$, which represents the degeneracy situation of the TPM. To find the regularity of the original TPM's distribution by columns, we transpose M_d to M_d^T , which is normalized by the $dg_vector = [0, 2, 1, 1]$ to derive the $M_{dnormal}^T$.

$$M_{dnormal}^T = \frac{M_d^T}{dg_vector} = \begin{bmatrix} 0 & 0 & 0 & 0 \\ \frac{1}{2} & 0 & 0 & \frac{1}{2} \\ 0 & 1 & 0 & 0 \\ 0 & 0 & 1 & 0 \end{bmatrix}$$

Based on this process, the question "what is the general regularity in M_d 's distribution by columns?" is transferred to "what is the general regularity in $M_{dnormal}^T$'s distribution by rows?". The former question is hard to answer as the layout of the TPM with x polynomial elements is stochastic, such as the M_d^x 's displays. On the contrary, the distribution by the $M_{dnormal}^T$'s rows tends to be more relative to the settings of hyperparameters, $future_dg_num$ and dg_level .

$$M_{d1}^x = \begin{bmatrix} x(1-x) & x^2 & (1-x)^2 & x(1-x) \\ x(1-x) & (1-x)^2 & x^2 & x(1-x) \\ (1-x)^2 & x(1-x) & x(1-x) & x^2 \\ x(1-x) & x^2 & (1-x)^2 & x(1-x) \end{bmatrix}$$

where $future_dg_num = 1$ and $dg_level = 2$

$$M_{d2}^x = \begin{bmatrix} x(1-x) & x^2 & (1-x)^2 & x(1-x) \\ (1-x)^2 & x(1-x) & x(1-x) & x^2 \\ (1-x)^2 & x(1-x) & x(1-x) & x^2 \\ x(1-x) & x^2 & (1-x)^2 & x(1-x) \end{bmatrix}$$

where $future_dg_num = 2$ and $dg_level = 4$

4.1.2 Numerical Method

Numerical Method wants to find the relationship between the degeneracy and the CE uncertainty threshold based on the experiment results in Figure 12. With the quantification by Equation 14, the approximate CE uncertainty thresholds are 0.2647 for the intersection between the cyan curve and the red line, 0.2332 for the intersection between the pink curve and the red line, and 0.1982 for the intersection between the green curve and the red line. The drop rate of the CE uncertainty threshold is nearly constant with the increasement of the degeneracy. Therefore, the regularity in Figure 12 could be used to derive the relationship between two hyperparameters, $future_dg_num$ and dg_level , and the CE uncertainty thresholds.

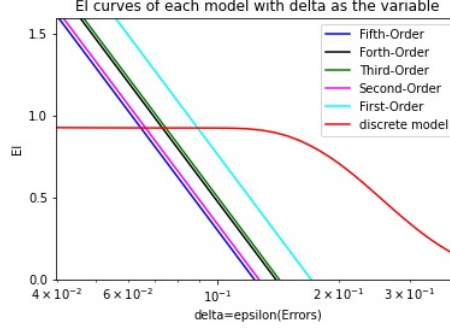


Figure 13: EIs of Five Continuous Models and One-Variable Discrete Model with the Continuous Uncertainty, δ and ϵ . The mapping trajectories of six models are shown in Figure 2.

4.2 Causal Emergence In Systems with Continuous States

As the common representation of numerous practical systems, it is necessary to discuss the CE in a model with continuous states. Through Equation 5, we have reproduced the EIs of five micro models with continuous states and the one-variable discrete-state macro model with the continuous uncertainty represented by δ and ϵ . In Figure 13, the CE uncertainty threshold relates to the complexity of the micro models. There is the largest CE uncertainty threshold while squeezing the simplest micro model to the macro, as shown by the intersection between the cyan curve and the red curve. The next step is to quantify the CE uncertainty threshold and discuss the factor that changes the threshold's value.

In 2022, Zhang and Liu quantified the relationship between the CE and the model's continuous states and proposed the Neural Information Squeezer framework to find the effective model-squeezing method from the time-series data[25]. The limitation of their research is, the CE will happen unconditionally in the process of squeezing the micro model to the macro model, which does not match our experiment results. Therefore, the CE uncertainty thresholds could be quantified through the relationship raised in [25], and then the more practical CE conditions can be identified. Consequently, The model's performance and potential optimization methods could be evaluated by its uncertainty and properties instead of some kinds of metrics.

5 Conclusion

In this paper, we proposed uncertainty redistribution as the deterministic factor of the CE by squeezing the micro models to the macro model. We also developed the General EI Calculator based on Equations 1, 2, and 3 and derived the CEQE in Equation 11 from the TPM's distribution by row, as shown by Equation 7. According to the experiment results displayed by Figures 6, 7, and 8, the CE uncertainty thresholds quantified by Equation 11 proved the CE has to satisfy two conditions: Firstly, the micro model's uncertainty has to be greater than the CE uncertainty threshold. Secondly, the micro model's uncertainty has to be redistributed to the specific range of the macro model's uncertainty.

In addition, we have raised Equation 13 and discussed the degeneracy as the CE factor in Experiments 2 and 3 respectively. For the model with multiple uncertainty variables $X = \{x_1, x_2, \dots, x_n\}$, the effect of one variable $x_i \in X$ attenuates to $\frac{a_i}{n}$ of the unified uncertainty x_u 's effect, as shown in Figure 10. The conditions of the CE are summarized by Proposition 5. These results further approved the uncertainty distribution as the general factor of the CE by coarse-graining the discrete micro model to the macro model, which is more effective and explainable.

Based on the total experiment results, there exists a potential space that contains numerous macro models which satisfy the CE conditions. The model with less uncertainty and degeneracy is more appropriate for the CE by squeezing the micro model. The conclusion is, the uncertainty and degeneracy are a type of error that decreases the model's EI. The uncertainty influences the model's effectiveness, and the degeneracy affects the model's explainability. Therefore, we assume the nature of causality is comprehensive quantification of the model's advantages. The nature of causal emergence should be the model's error declines by the coarse-graining following the assumption above.

For future studies, the mathematical expression of degeneracy can be derived, and the CE conditions of the model with continuous states can be discussed. To deal with the complexity of calculating the EI by the TPM, Algebraic Method and Numerical Method can be researched to derive the degeneracy expression. Another interesting topic is to extend

the CE conditions to more practical scenario, which is the model with continuous states: the CE conditions of the continuous uncertainty and the micro model's properties could be verified based on Zhang and Liu's work[25].

Acknowledgement

This work is partially supported by the Xi'an Jiaotong-Liverpool University(XJTLU) AI University Research Centre, Jiangsu (Provincial) Data Science and Cognitive Computational Engineering Research Centre at XJTLU; and research funding: XJTLU-REF-21-01-002.

This research received financial support from Jiangsu Industrial Technology Research Institute (JITRI) and Wuxi National Hi-Tech District (WND). This research received no third-party funding.

Author Contributions

research ideas, Y. Y.; method, experiment and analysis, L. J.; supervision, Y.Y., K.L.M., J.S., and S. G.; writing, original draft, L. J.; writing, review and editing, C. Z. and Y.Y. All authors read and agreed to the published version of the manuscript.

References

- [1] Seth Lloyd. Computational capacity of the universe. *Physical Review Letters*, 2002.
- [2] Yutao Yue. A world-self model towards understanding intelligence. 2022.
- [3] Judea Pearl and Dana Mackenzie. The book of why: The new science of cause and effect. 2018.
- [4] Pavel Chvykov and Erik Hoel. Causal geometry. *arXiv: Information Theory*, 2020.
- [5] Karl E. Case. Principles of microeconomics, 12/e. 2020.
- [6] A. Einstein. Über einen die erzeugung und verwandlung des lichtetes betreffenden heuristischen gesichtspunkt. *Annalen der Physik* 4, 1905.
- [7] S. Pepper. Emergence. *Journal of Philosophy* 23 241-245, 1926.
- [8] Yaneer Bar-Yam. A mathematical theory of strong emergence using multiscale variety. *Complexity* 9(6): 15-24, 2004.
- [9] Philip W. Anderson. More is different: Broken symmetry and the nature of the hierarchical structure of science. 1972.
- [10] Brennan Klein and Erik Hoel. Uncertainty and causal emergence in complex networks. 2019.
- [11] Umut Baysan. Causal emergence and epiphenomenal emergence. *Erkenntnis*, 2020.
- [12] Judea Pearl. Causality: models, reasoning, and inference. *Tijdschrift Voor Filosofie*, 2009.
- [13] Sophia Kivelson and Steven A. Kivelson. Defining emergence in physics. *npj Quantum Materials*, 2016.
- [14] Jochen Fromm. Types and forms of emergence. *arXiv: Adaptation and Self-Organizing Systems*, 2005.
- [15] Erik Hoel, Larissa Albantakis, and Giulio Tononi. Quantifying causal emergence shows that macro can beat micro. *Proceedings of the National Academy of Sciences of the United States of America*, 2013.
- [16] Daniel P. Buxhoeveden and Manuel F. Casanova. The minicolumn hypothesis in neuroscience. *Brain*, 125:935–951, 2002.
- [17] Jon H. Kaas. Why does the brain have so many visual areas. *Journal of Cognitive Neuroscience*, 1:121–135, 1989.
- [18] Claudio Galletti, Patrizia Fattori, Michela Gamberini, and Dieter F. Kutz. The cortical visual area v6: brain location and visual topography. *European Journal of Neuroscience*, 11:3922–3936, 1999.
- [19] Erik Hoel. When the map is better than the territory. *Entropy*, 2017.
- [20] Renzo Comolatti and Erik Hoel. Causal emergence is widespread across measures of causation. 2022.
- [21] Thomas Varley and Erik Hoel. Emergence as the conversion of information: A unifying theory. *arXiv: Information Theory*, 2021.
- [22] David Balduzzi. Information, learning and falsification. *arXiv preprint arXiv:1110.3592*, 2011.
- [23] Shun-ichi Amari. *Information geometry and its applications*, volume 194. Springer, 2016.

- [24] Fernando E Rosas, Pedro AM Mediano, Henrik J Jensen, Anil K Seth, Adam B Barrett, Robin L Carhart-Harris, and Daniel Bor. Reconciling emergences: An information-theoretic approach to identify causal emergence in multivariate data. *PLoS computational biology*, 16(12):e1008289, 2020.
- [25] Jiang Zhang. Neural information squeezer for causal emergence. *arXiv preprint arXiv:2201.10154*, 2022.